Absolute flatness measurement using oblique incidence setup and an iterative algorithm. A demonstration on synthetic data

Maurizio Vannoni*

European XFEL GmbH, Albert-Einstein-Ring 19,22761 Hamburg, Germany
maurizio.vannoni@xfel.eu

Abstract: A method to provide absolute planarity measurements through an interferometric oblique incidence setup and an iterative algorithm is presented. With only three measurements, the calibration of absolute planarity is achieved in a fast and effective manner. Demonstration with synthetic data is provided, and the possible application to very long flat mirrors is pointed out.

OCIS codes: (120.0120) Instrumentation, measurement, and metrology; (120.3180) Interferometry; (120.3940) Metrology; (120.4800) Optical standards and testing; (120.6650) Surface measurements, figure.

References and links

1. M. Zeuner and S. Kiontke, "Ion beam figuring technology in optics manufacturing," Optik & Photonik **7**(2), 56–58 (2012).
2. M. Weiser, "Ion beam figuring for lithography optics," Nucl. Instrum. Methods Phys. Res. B **267**(8-9), 1390–1393 (2009).
3. J. Arkwright, J. Burke, and M. Gross, "A deterministic optical figure correction technique that preserves precision-polished surface quality," Opt. Express **16**(18), 13901–13907 (2008).
4. A. Schutze, J. Y. Jeong, S. E. Babayan, and J. Park, "The atmospheric-pressure plasma jet: a review and comparison to other plasma sources," IEEE Trans. Plasma Sci. **26**(6), 1685–1694 (1998).
5. T. Arnold, G. Böhm, R. Fechner, J. Meister, A. Nickel, F. Frost, T. Hänsel, and A. Schindler, "Ultra-precision surface finishing by ion beam and plasma jet techniques—status and outlook," Nucl. Instrum. Meth. A **616**(2-3), 147–156 (2010).
6. Y. Mori, K. Yamauchi, and K. Endo, "Elastic emission machining," Precis. Eng. **9**(3), 123–128 (1987).
7. S. Matsuyama, T. Wakioka, N. Kidani, T. Kimura, H. Mimura, Y. Sano, Y. Nishino, M. Yabashi, K. Tamasaku, T. Ishikawa, and K. Yamauchi, "One-dimensional Wolter optics with a sub-50 nm spatial resolution," Opt. Lett. **35**(21), 3583–3585 (2010).
8. W. Gao, P. S. Huang, T. Yamada, and S. Kiyono, "A compact and sensitive two-dimensional angle probe for flatness measurement of large silicon wafers," Precis. Eng. **26**(4), 396–404 (2002).
9. M. Schulz and C. Elster, "Traceable multiple sensor system for measuring curved surface profiles with high accuracy and high lateral resolution," Opt. Eng. **45**(6), 060503 (2006).
10. R. D. Geckeler, "Optimal use of pentaprism in highly accurate deflectometric scanning," Meas. Sci. Technol. **18**(1), 115–125 (2007).
11. P. C. V. Mallik, C. Zhao, and J. H. Burge, "Measurement of a 2m flat using a pentaprism scanning system," Opt. Eng. **46**, 023602 (2007).
12. F. Siewert, J. Buchheim, S. Boutet, G. J. Williams, P. A. Montanez, J. Krzywinski, and R. Signorato, "Ultra-precise characterization of LCLS hard X-ray focusing mirrors by high resolution slope measuring deflectometry," Opt. Express **20**(4), 4525–4536 (2012).
13. J. Yellowhair and J. H. Burge, "Analysis of a scanning pentaprism system for measurements of large flat mirrors," Appl. Opt. **46**(35), 8466–8474 (2007).
14. J. Ojeda-Castañeda, "Foucault, wire and phase modulation tests," in *Optical Shop Testing*, third edn., D. Malacara ed., (Wiley and Sons, Hoboken 2007), pp. 310–312.
15. L. Rayleigh, "Interference bands and their applications," Nature **48**(1235), 212–214 (1893).
16. B. S. Fritz, "Absolute calibration of an optical flat," Opt. Eng. **23**(4), 234379 (1984).
17. R. E. Parks, L.-Z. Shao, and C. J. Evans, "Pixel-based absolute topography test for three flats," Appl. Opt. **37**(25), 5951–5956 (1998).
18. M. F. Küchel, "A new approach to solve the three flat problem," Optik (Stuttg.) **112**(9), 381–391 (2001).
19. U. Griesmann, Q. Wang, and J. Soons, "Three-flat tests including mounting-induced deformations," Opt. Eng. **46**(9), 093601 (2007).

#200810 - $15.00 USD Received 6 Nov 2013; revised 9 Jan 2014; accepted 10 Jan 2014; published 6 Feb 2014

20. V. Greco and G. Molesini, "Micro-temperature effects on absolute flatness test plates," Pure Appl. Opt. **7**(6), 1341–1346 (1998).
21. V. Greco, R. Tronconi, C. Del Vecchio, M. Trivi, and G. Molesini, "Absolute measurement of planarity with Fritz's method: uncertainty evaluation," Appl. Opt. **38**(10), 2018–2027 (1999).
22. L. Zhang, B. Xuan, and J. Xie, "Combination of skip-flat test with Ritchey-Common test for the large rectangular flat," Proc. SPIE **7656**, 76564W (2010).
23. P. Hariharan, "Interferometric testing of optical surfaces: absolute measurements of flatness," Opt. Eng. **36**(9), 2478–2481 (1997).
24. D. Malacara, "Twyman-Green interferometer," in *Optical Shop Testing*, third edn., D. Malacara ed., (Wiley and Sons, Hoboken 2007), pp. 78–79.
25. Z. Han, L. Chen, T. Wulan, and R. Zhu, "The absolute flatness measurements of two aluminum coated mirrors based on the skip flat test," Optik (Stuttg.) **124**(19), 3781–3785 (2013).
26. M. Vannoni, A. Sordini, and G. Molesini, "Calibration of absolute planarity flats: generalized iterative approach," Opt. Eng. **51**(8), 081510 (2012).
27. V. B. Gubin and V. N. Sharonov, "Algorithm for reconstructing the shape of optical surfaces from the results of experimental data," Sov. J. Opt. Technol. **57**, 147–148 (1990).
28. M. Vannoni and G. Molesini, "Iterative algorithm for three flat test," Opt. Express **15**(11), 6809–6816 (2007).
29. M. Vannoni and G. Molesini, "Absolute planarity with three-flat test: an iterative approach with Zernike polynomials," Opt. Express **16**(1), 340–354 (2008).
30. M. Vannoni and G. Molesini, "Three-flat test with plates in horizontal posture," Appl. Opt. **47**(12), 2133–2145 (2008).
31. C. Morin and S. Bouillet, "Absolute calibration of three reference flats based on an iterative algorithm: study and implementation," Proc. Soc. Photo Opt. Instrum. Eng. **8169**, 816915 (2011).
32. M. Vannoni, A. Sordini, and G. Molesini, "Long-term deformation at room temperature observed in fused silica," Opt. Express **18**(5), 5114–5123 (2010).
33. M. Vannoni, A. Sordini, and G. Molesini, "Relaxation time and viscosity of fused silica glass at room temperature," Eur Phys J E Soft Matter **34**(9), 92 (2011).

1. Introduction

A traditionally important task for optical metrology laboratories is the absolute shape characterization of planarity standards. This capability is even more important today, as many research projects are pushing further the optical quality specifications, often requiring an accuracy of few nanometers peak-to-valley on the entire clear aperture. These highly demanding specifications are currently approached using deterministic polishing, as ion-beam figuring [1–3], atmospheric plasma-jet surface processing [4,5], and elastic-emission-machining [6,7]. The availability of these advanced polishing methods has reinforced the connection between manufacturing and surface metrology. Actually, deterministic polishing is mostly used in two different cases: for free-form and aspheric surfaces, to manufacture mirrors with shapes that cannot be obtained with standard polishing, and for standard surfaces, like flat or spherical, if a particularly high accuracy is required. A common procedure to prepare such high quality optical surfaces is to make preliminarily a standard polishing. After that, the surface is measured with the greatest accuracy and the resulting profile is used as an input for the deterministic polishing process. In such a way, the surface is locally adjusted and, after that, it is generally measured again to check the final quality achieved. The deterministic polishing and the measuring operations can be repeated in a cycle until the specifications are satisfied.

Understandably, the resulting manufacturing process is lengthy and expensive. In fact, the time necessary for each polishing has to be multiplied times the number of cycles needed to reach the desired results. Another hindrance is the limited spatial resolution of the particular process used for deterministic polishing itself, not permitting to precisely intervene on the defects to be corrected. But the main problem is still the metrological connection between the measurements and the polishing process. In order to optimize the entire process, the possibility to carry out fast and accurate surface measurements in an absolute way is still critical since it affects directly the final surface quality that can be obtained.

New measuring approaches based on laser deflectometry are under way to development and validation [8–13]; classically, high accuracy surface measurements are performed using Fizeau interferometers. However, interferometers compare a test surface with a reference one,

#200810 - $15.00 USD Received 6 Nov 2013; revised 9 Jan 2014; accepted 10 Jan 2014; published 6 Feb 2014

allowing in this way just relative measurements. If the quality required for the test surface is close to or even better than that of the reference surface, an absolute method should be used.

A classical method to perform absolute planarity measurements of large flat mirrors is by the Ritchey-Common test [14]. For this purpose, a good spherical mirror is used, with a pinhole source at the center of curvature, so that an absolute reference cavity is defined. The flat mirror to be tested is inserted at oblique incidence between the pinhole and the spherical mirror, bending the optical configuration. The inspection of the focal distribution with a knife-edge device allows to detect the departures from planarity of the test mirror.

The availability of modern interferometers has now eased the task of absolute planarity measurements; the most used method is the three-flat test [15–19]. Three nominally flat surfaces are examined with a Fizeau interferometer, comparing each other in a particular sequence. The interferograms are then processed taking into account the measuring sequence, and the absolute shape of all the three flats is ideally worked out. The method has been widely developed and used with different setups and data processing schemes. However, using just three measurements and a closed, analytical calculation, the method only provides the absolute profile along one surface diameter. If additional measurements are performed, including azimuthal rotations of the flats, different mathematical elaborations can be used, so that more diameters or even the whole surface can be retrieved. To get the surface shape of all the three surfaces, a minimum of four measurements is required. The reconstruction of the entire surfaces is anyway affected by at least two basic assumptions that need to be considered when the measurement results are evaluated. The first assumption is that the surfaces are fairly regular and free of local defects; this is particularly important when shape retrieval is based upon fitting orthogonal polynomials to the interferometric data, since such an operation generally wipes out the high spatial frequency features of the surfaces [16]. The second assumption is that the surfaces are not changing their shape through the different steps of the measuring sequence, although the flats are moved to different positions where they undergo to different mechanical and thermal constraints [20,21]. For these reasons, slight departures between the calculated shapes and the real ones are possible, so limiting the actual level of the final accuracy. Avoiding polynomial fitting, and using a reduced set of measurements with a setup where the flats do not need to be moved to different mountings, could be a key factor to effectively improve the accuracy, in particular for large optics.

We here propose a modified three-flat test in which we retrieve the entire surface shape of one of the three flats using just three measurements and without removing the optics from their mechanical mountings. Data are analyzed using a pixel-based iterative algorithm not requiring polynomial fitting. The optics concept of the experimental setup is presented, and simulated data are produced and then processed to discuss the expected accuracy of the measuring chain. Such a method could be effectively used for large flats, and in particular for long mirrors used in synchrotrons or free electron laser beamlines.

2. Oblique incidence setup

The so called “oblique incidence setup”, or also “skip-flat test”, is a common method among optics manufacturers to test large flats [22–24]. The method has been also very recently reported [25], with two different setups to retrieve the surface figure of the flat mirror through Zernike polynomials decomposition.

The basic system is provided by a standard Fizeau interferometer, equipped with a transmission flat (here named K) and a reference flat (here named M). The flats K and M are used to define a measurement cavity where the test surface (here named L) is inserted at a certain incidence reflecting angle α [Fig. 1(a)]. The setup is on the horizontal plane, putting L, K and M surfaces along the vertical, to minimize deformations due to gravity. After the measurement with L in place, the cavity itself is measured removing L and realigning K and M in front of each other [Fig. 1(b)]. The latter measurement is then repeated rotating the flat M

#200810 - $15.00 USD Received 6 Nov 2013; revised 9 Jan 2014; accepted 10 Jan 2014; published 6 Feb 2014

on its plane through an angle β [Fig. 1(c)], so that information on the azimuthal error of the cavity is also acquired.

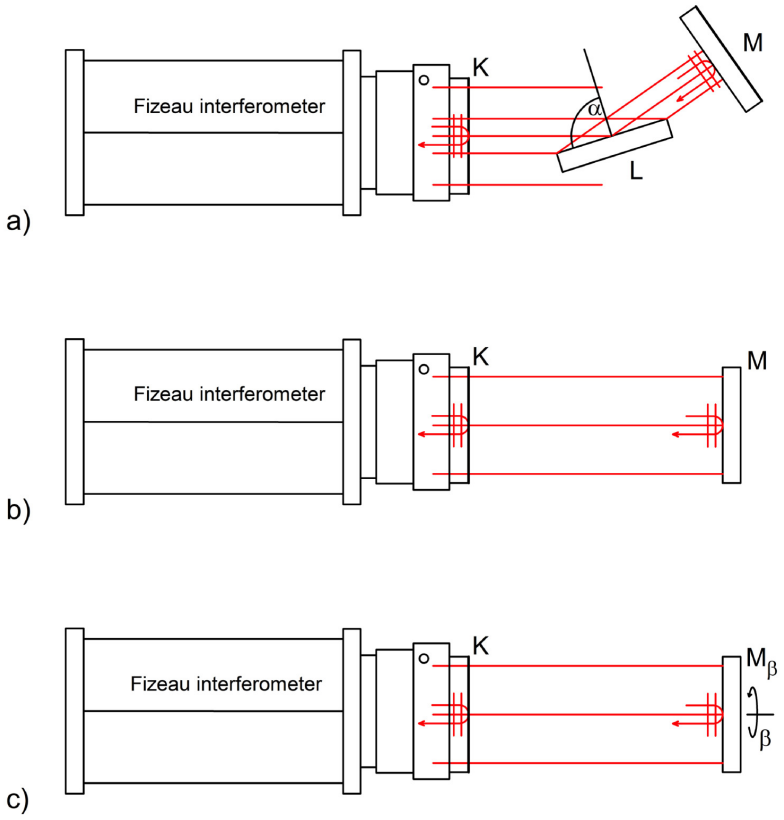

Fig. 1. Optical setup and measuring steps for absolute flatness measurement: (a), cavity including the test surface; (b), cavity in the absence of the test surface; (c), same cavity with the reference flat *M* rotated on its plane.

We indicate the planarity error of the three surfaces by the name of the flats they belong to, namely, $K(x,y)$, $M(x,y)$ and $L(x,y)$, with (x, y) the local coordinates of each surface. Referring to the sequence (a), (b), (c) in Fig. 1, we also indicate the maps of optical path difference (*OPD*) measured with the interferometer as $KLM(x,y)$, $KM(x,y)$, $KM_\beta(x,y)$, respectively. To represent the measuring configurations and the posture of the flats in each step, we introduce a set of operators acting on the data maps or the surface coordinates [26]; in particular we use the operators listed in Table 1.

Table 1. Operators acting on the flats and accounting for the data maps

Symbol	Description
F_y	"flip" about the *y*-axis
$F_y^{-1} = F_y$	undo the *y*-flip
R_β	azimuthal rotation by an angle β
$R_\beta^{-1} = R_{(2\pi-\beta)}$	azimuthal counter-rotation by an angle β
$S_{y,\alpha}$	tilt about the local *y*-axis by an angle α, with scaling factor taken in account

#200810 - $15.00 USD Received 6 Nov 2013; revised 9 Jan 2014; accepted 10 Jan 2014; published 6 Feb 2014

All such operators correspond to actions imparted to the flats at the data acquisition stage, and have a counterpart in software routines that are applied to the data during the subsequent processing stage. Considering for example the rotation of the flat M through an angle β as in Fig. 1(c), the result is represented with $R_\beta M$. The operators above are linear, but do not commute: they must be applied in the proper order. We have therefore

$$KLM(x,y) = F_y K + S_{y,\alpha} L + F_y M \tag{1}$$

$$KM(x,y) = F_y K + M \tag{2}$$

$$KM_\beta(x,y) = F_y K + R_\beta M \tag{3}$$

The operator $S_{y,\alpha}$ is specific to the oblique incidence setup; applied to the tilted surface L, it represents the fact that such surface seen from the beam is stretched along the x-axis; also, the height is multiplied times a scaling factor depending on the angle α . As to the latter factor, it includes two different effects, as shown in Fig. 2 where a height step Δz is drawn: the first effect is that the *OPD* changes from $2\Delta z$ to $2\cos\alpha\ \Delta z$; the second effect is a further factor of two due to double pass, so that the overall scaling factor with respect to the case of normal incidence is $2\cos\alpha$. In detail, being (i, j) the matrix indices of the current element, and (i_0, j_0) the indices of the central element, the operator $S_{y,\alpha}$ is defined by the expression

$$S_{y,\alpha} L(i,j) = 2\cos\alpha \cdot L\left[(i - i_0)\cos\alpha + i_0, j\right] \tag{4}$$

If $\alpha \le 60$ degrees, the scaling factor is equal to or greater than unity, so the sensitivity of the setup is the same or even higher compared to normal incidence.

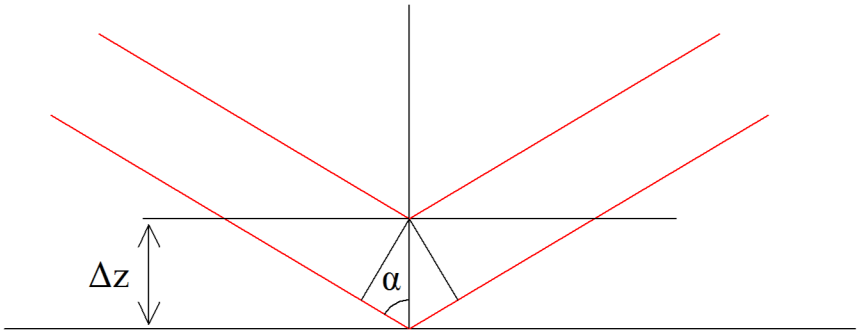

Fig. 2. Optical path difference $2\cos\alpha\ \Delta z$ introduced on oblique reflection by a step of height Δz.

The operator F_y applied to M in Eq. (1) is because the beam impinging on M is mirrored by the surface L about the y-axis, then causing a reversal of the x-coordinates on the *OPD* introduced by M. Naturally, in Eq. (2) relating to the case of empty cavity such a reversal is not occurring, and F_y is not intervening. As to the azimuthal rotation angle β in Eq. (3), its value should be selected avoiding integer sub-multiples of 360 degrees [26]; the optimum value suggested in the literature and widely used in practice is $\beta = 54$ degrees [27].

To simulate the setup, we generated three synthetic maps corresponding to K, L and M using a random selection of low spatial frequency Zernike polynomials. To better account for real experimental conditions, we also added a Gaussian distribution of white noise. We then computed the interference patterns $KLM(x,y)$, $KM(x,y)$, $KM_\beta(x,y)$ that would be produced in the measuring sequence of Fig. 1. As an example, here we report the results we obtained using a selection of low spatial frequency terms with 100 nm Peak-to-Valley (P-V) and 10 nm root-

#200810 - $15.00 USD Received 6 Nov 2013; revised 9 Jan 2014; accepted 10 Jan 2014; published 6 Feb 2014

mean-square (rms), and a white noise with 25 nm P-V and 2.5 nm rms. We set α = 45 degrees and β = 54 degrees. In Fig. 3 we present the expected measurement results according to Eqs. (1)-(3).

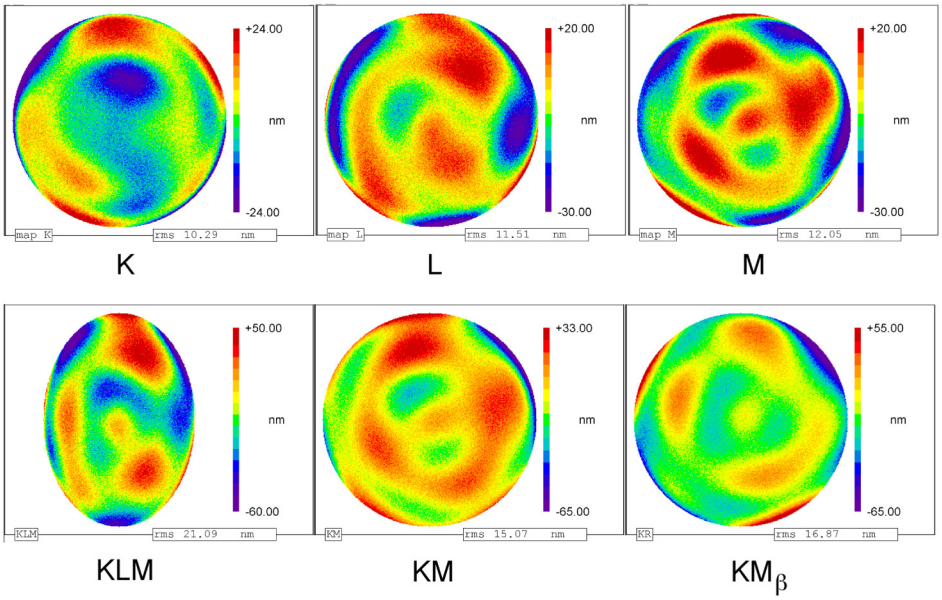

Fig. 3. Example of synthetic surfaces *K*, *L*, *M* and simulated OPD maps *KLM*, *KM*, KM_β.

Because of the oblique incidence setup, the map *KLM* appears laterally compressed. In fact, if the dimensions of all the three flats are the same, the surfaces *K* and *M* are vignetted by *L*. If the flat *L* has an elliptical footprint, the tilt angle α could be adjusted to minimize the compression effect, then improving the spatial resolution and the sensitivity. It is understood that in real measurements the tilt angle needs be optimized depending on the size and shape of the test surface *L*. For that reason, final results cannot be easily retrieved with standard data processing. To have a procedure reliable and easy to be optimized, we here present a data processing approach based on an iterative algorithm [28,29]. The latter has been already used with standard three-flat setup, both in horizontal and in vertical configurations, showing clear advantages as to versatility and effectiveness [30,31]; it was also used in the area of applied research, where it allowed to observe the viscoelastic behavior of fused silica glass at room temperature [32,33]. In the present case, the iterative algorithm is used to retrieve the absolute figure of the test surface *L* with pixel resolution and sub-nanometric rms accuracy.

3. Data processing with Iterative Algorithm

Firstly we calculate the difference between *KLM* and *KM*:

$$KLM(x,y) - KM(x,y) = S_{y,\alpha}L + F_y M - M \qquad (5)$$

The figure map of *M* can be divided in two separate contributions: a rotationally invariant part, as spherical aberration, and a rotation dependent part, as astigmatism or cylinder. The rotationally invariant part is also mirror invariant, so it is automatically cancelled in Eq. (5) by the difference $F_y M - M$. What remains is due to the rotation dependent part only. Such part can be retrieved building up an iterative algorithm with *KM* and KM_β as inputs. To this purpose, the following steps are implemented:

#200810 - $15.00 USD Received 6 Nov 2013; revised 9 Jan 2014; accepted 10 Jan 2014; published 6 Feb 2014

1. Generate an initial set of trial surfaces K and M (they can be created randomly or also initially taken as a matrix of zeroes).

2. Compute the maps of the synthetic measurement KM and KM_β using Eqs. (2) and (3).

3. Evaluate the differences $\Delta(KM)$ and $\Delta(KM_\beta)$ between KM and KM_β and the corresponding real measurement $(KM)_{exp}$ and $(KM_\beta)_{exp}$ obtained in experiments:

$$\Delta(KM) = (KM)_{\text{exp}} - KM \quad , \tag{6}$$

$$\Delta(KM_\beta) = (KM_\beta)_{\text{exp}} - KM_\beta \quad . \tag{7}$$

4. Undo the operators, i.e., unflip or counter-rotate the differences maps where necessary, scale down (here by a factor of 10) and share the differences among K and M to obtain new values K_{new}, M_{new}:

$$K_{\text{new}} = K + \frac{1}{2}\frac{1}{10}F_y\Delta(KM) + \frac{1}{2}\frac{1}{10}F_y\Delta(KM_\beta) \quad , \tag{8}$$

$$M_{\text{new}} = M + \frac{1}{2}\frac{1}{10}\Delta(KM) + \frac{1}{2}\frac{1}{10}R_\beta^{-1}\Delta(KM_\beta) \quad . \tag{9}$$

5. Update the maps replacing K and M with K_{new}, M_{new} and go back to step 2. The cycle exits if the rms values of the difference $\Delta(KM)$ and $\Delta(KM_\beta)$ computed in step 3 reach a minimum or become smaller than a given threshold. We can also set the cycle to be repeated for a fixed number of times.

Applying such an iterative algorithm to the example presented in Fig. 3, we retrieve the maps of K and M shown in Fig. 4. Computing the differences between the retrieved maps and the starting ones, we can clearly see that the angular part is fully reconstructed while the rotationally invariant part is not: however, since we are going to use Eq. (5) where the latter is automatically discarded, this missing reconstruction has no consequences.

Using then the retrieved map M, we now calculate the angular part $\left(F_yM - M\right)$, and the stretched map $S_{y,\alpha}L$ with Eq. (5):

$$S_{y,\alpha}L = KLM - KM - (F_yM - M) \quad . \tag{10}$$

To finally get L, in principle we could define and use an inverse operator $S_{y,\alpha}^{-1}$, undoing the stretching and scaling operated by $S_{y,\alpha}$. Initially however, when we computed KLM, we stretched L and so we lost some lateral resolution. This naturally occurs also in real measurements, looking at L with an oblique incidence angle. So, to evaluate the algorithm in itself we here do not consider lateral resolution, limiting ourselves to undo the scaling only. The result is shown in Fig. 4, where the retrieved surfaces K, L (stretched), M are presented, along with the pertaining error maps. Remarkably, while significant (basically, rotation invariant) errors on K and M are still present, the oblique map of L is retrieved with sub-nanometric rms accuracy.

#200810 - $15.00 USD Received 6 Nov 2013; revised 9 Jan 2014; accepted 10 Jan 2014; published 6 Feb 2014

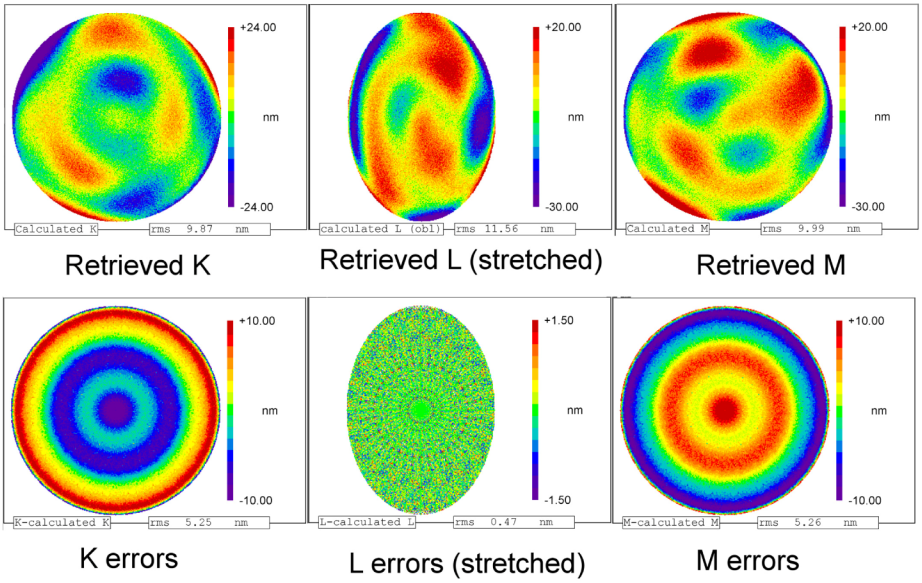

Fig. 4. Retrieved surfaces *K*, *L* (oblique), *M*, after the application of the iterative algorithm. The error maps with respect to the starting surfaces are also presented.

4. Application to mirrors with elliptical footprint

As we have seen, the most important inconvenience in retrieving the absolute surface figure of a flat with the oblique incidence setup is the reduced lateral resolution along the surface length. On the other hand, in some cases we have surfaces (particularly mirrors) that are longer in one dimension than in the other, and it is required to optimize the measuring setup to ensure the maximum resolution. Considering for example a mirror with elliptical footprint, major axes *X* and *Y*, with $X > Y$: if the diameter of the laser beam out of the interferometer is *D*, with $D < X$, a tilt angle $\alpha = \arcsin(D/X)$ still allows to measure the entire mirror with the best resolution.

The accuracy of the iterative algorithm in itself is not affected by the tilt angle, because the method is used to recover *K* and *M* from *KM* and KM_β maps, not including any oblique incidence measurements. For this reason, the theoretical accuracy of the measurement only depends on the uncertainty of the scaling factor and on the intrinsic errors of the stretching effect. While the latter is unavoidable, the former is changing with the tilt angle, resulting in a desensitization of the method when such an angle is increased. If we take the rms error 0.47 nm with a 45 degrees angle, as with our data, and assume that such a quantity is proportional to the scaling factor, we have the straightforward expression

$$\mathrm{rms}(\alpha) = \frac{\cos(\pi/4)}{\cos\alpha}\ 0.47\ \mathrm{nm} = \frac{X}{D}\frac{\sqrt{2}}{2}\ 0.47\ \mathrm{nm}\,. \qquad (11)$$

To a numerical example, considering a beam diameter D = 300 mm and an elliptical mirror with major axis X = 800 mm, the measuring approach here described is expected to achieve an accuracy of approximately 0.9 nm rms, still at a subnanometer level.

5. Other error sources

When the described procedure is used on experimental data, we would expect also other sources of error to affect the measurement. Small discrepancies on the tilt angle could impair the algorithm performance, introducing a mismatch between the corresponding pixel maps.

#200810 - $15.00 USD Received 6 Nov 2013; revised 9 Jan 2014; accepted 10 Jan 2014; published 6 Feb 2014

Moreover, small misalignments of the flats could affect the pixel-by-pixel approach of the method. Based on our experimental experience, repositioning errors should be negligible in the *KM* and KM_β measurements: the flats are not displaced but only rotated, and a mechanical reference can be used to avoid mismatches between the two measurements. The measurement *KLM* is instead more critical: the tilted surface is cropping the beam, so that we have fewer fiducial references, and small misalignments are more likely to occur. To quantify the influence of these effects, we made some simulations.

For the tilt angle, we introduced a ± 1 degrees difference on the α-value used to generate the *KLM* synthetic map; after that, we applied the iterative algorithm, assuming that we still had a tilt angle of exactly 45 degrees. The error computed on the difference map between the retrieved *L*-map and the original one so becomes 0.57 nm rms, slightly larger than previously.

We now consider the possible misalignments of the flats when the measurement *KLM* is made. During all the procedure, the flat *K* is remaining attached to the Fizeau interferometer, so we can assume that its correspondence to the pixels matrix is fixed. The flat *L* is used in this measurement for the first time, so repositioning errors are not occurring. The position of the flat *M* is more critical because it is realigned to fit the tilt angle setup: it is possible to have some mismatch between the actual pixel map and the one considered in the other measurements, in particular if *L* is small and most of the beam is vignetted. Such a mismatch can be reduced to the pixel level using proper alignment aids, for example introducing fiducial masks to identify the center of each surface. Based on these considerations, we made a simulation imparting to the flat *M* a misalignment of ± 1 pixel along the *x* and *y* axes. Working out the map of residuals between the retrieved flat *L* and the original one, typical values of 2.6 nm rms error are found. This relatively large error is mostly originated from the distribution of white noise considered in this example, creating high spatial frequency residuals that cannot be retrieved with even a small mismatch. This effect is generally present in every three-flat data-retrieving algorithm. If we repeat this simulation using maps with a ten times lower noise level, we find a maximum value of 0.64 nm rms on the *L*-map residual error.

In the light of the above simulations, it appears that the errors expected in experiments could be reduced to a level comparable with the accuracy of the data processing algorithm, by keeping the signal-to-noise level sufficiently low and minimizing the misalignment of the flats.

6. Conclusions

A method to measure the absolute planarity of optical flats with an oblique incidence setup and the use of an iterative algorithm has been described. Simulation of the measuring chain on synthetic surface data has been provided, showing the capability of the approach to achieve an accuracy of the order of the nanometer rms (or even smaller than that, depending on the angle of incidence of the probe beam on the test surface).

For its implementation, the method relates to the use of few operators acting on the data maps provided by a Fizeau interferometer in the course of only three measurements, without having to remove the flat under test from its mounting. The algorithm for data reduction is pixel-based, and does not imply any polynomial fitting, and then maintaining the resolution of the available hardware under the actual measuring conditions. Due to the limited number of measurements required and to the versatility and effectiveness of the data reduction processing, in addition to use for general metrology applications, the method is proposed as a resort of value particularly to assist the manufacture of high quality mirrors by deterministic polishing.

Acknowledgments

We would like to thank Dr. Harald Sinn and Dr. Giuseppe Molesini for useful discussions and suggestions.

#200810 - $15.00 USD Received 6 Nov 2013; revised 9 Jan 2014; accepted 10 Jan 2014; published 6 Feb 2014